Available online at www.sciencedirect.com

ScienceDirect

Rice Science, 2023, 30(5): 449−458

Research Paper

Effects of Zinc Oxide Particles with Different Sizes on Root Development in *Oryza sativa*

Monica RUFFINI CASTIGLIONE[1, 2, #], Stefania BOTTEGA[1, #], Carlo SORCE[1, 2], Carmelina SPANÒ[1, 2]

([1]*Department of Biology, University of Pisa, Via Luca Ghini, Pisa 13 56126, Italy;* [2]*Centre for Climate Change Impact, University of Pisa, Via del Borghetto, Pisa 80 56124, Italy;* [#]*These authors contributed equally to this work*)

Abstract: Given the consistent release of zinc oxide (ZnO) nanoparticles into the environment, it is urgent to study their impact on plants in depth. In this study, grains of rice were treated with two different concentrations of ZnO nanoparticles (NP-ZnO, 10 and 100 mg/L), and their bulk counterpart (B-ZnO) were used to evaluate whether ZnO action could depend on particle size. To test this hypothesis, root growth and development assessment, oxidative stress parameters, indole-3-acetic acid (IAA) content and molecules/enzymes involved in IAA metabolism were analyzed. *In situ* localization of Zn in control and treated roots was also performed. Though Zn was visible inside root cells only following nanoparticle treatment, both materials (NP-ZnO and B-ZnO) were able to affect seedling growth and root morphology, with alteration in the concentration/pattern of localization of oxidative stress markers and with a different action depending on particle size. In addition, only ZnO supplied as bulk material induced a significant increase in both IAA concentration and lateral root density, supporting our hypothesis that bulk particles might enhance lateral root development through the rise of IAA concentration. Apparently, IAA concentration was influenced more by the activity of the catabolic peroxidases than by the protective action of phenols.

Key words: zinc oxide; indole-3-acetic acid; lateral root; rice; bulk particle; nanoparticle

Zinc oxide nanoparticles (NP-ZnO), having useful properties such as ultraviolet-screening ability and photocatalytic and antibacterial activities (Pandimurugan and Thambidurai, 2016), are one of the most widely used nanoparticles in nanotechnological industries. Due to their wide range of applications in the production of paints, coatings, inks, plastics, cosmetics and personal care products, the annual production of these metal nanoparticles has reached 8 000 t (Vimercati et al, 2020). This high production and the wide use of NP-ZnO-containing products obviously increase the probability of leakage into the environment with increased possible risks for living organisms (Ma et al, 2013; Spanò et al, 2020; Rajput et al, 2021).

Despite many studies report a protective action of NP-ZnO on plants under stress conditions (Ali et al, 2019; Ali et al, 2022), some studies indicated a negative impact of NP-ZnO on plant growth (Zhang et al, 2015), in particular when its concentration is above a critical threshold (Srivastav et al, 2021). The phytotoxicity of these nanoparticles is not only attributable to the release of Zn^{2+} and its absorption by the roots (Ma et al, 2013; Mousavi Kouhi et al, 2015), but also to the nanoparticles themselves. NP-ZnO, in fact, can penetrate through cell wall pores if their dimensions are less than 30 nm or after eventual size reduction/decomposition of particles/aggregates (Molnár et al, 2020). Damages could be determined either by their direct interaction with biomolecules, with damage to membranes and/or DNA (Ma et al, 2013),

Received: 10 November 2022; **Accepted:** 8 March 2023

Corresponding author: Carlo SORCE (carlo.sorce@unipi.it)

Peer review under responsibility of China National Rice Research Institute

http://dx.doi.org/10.1016/j.rsci.2023.03.016

or by their ability to induce the generation of reactive oxygen species (ROS), such as hydrogen peroxide (H_2O_2) (Hernandez-Viezcas et al, 2011). In addition to the inhibition of seedling root growth, disturbances to root development have been recorded with damage/shortening of the root tip in NP-ZnO-treated ryegrass (Lin and Xing, 2008), and alteration in root morphology in wheat under treatment with both NP-ZnO and the bulk counterpart (Spanò et al, 2020).

The hypothesis has been made that this reshaping of root morphology could be mediated by the influence of Zn on the homeostasis of hormones, in particular of indole-3-acetic acid (IAA), which is pivotal in the regulation of root growth and lateral root (LR) development (Aloni et al, 2006; Alarcón et al, 2019). In fact, prominent is the role generally ascribed to this growth regulator in several biological processes (Lv et al, 2019), with biosynthesis and metabolism playing important functions in local auxin gradients, which are key factors for differentiation events (Overvoorde et al, 2010). In this study, grains of rice (*Oryza sativa* L.), commonly used as a model species for monocots and cereals in many morpho-physiological studies, were treated with two different concentrations of NP-ZnO (10 and 100 mg/L) and of their bulk counterpart (B-ZnO) particles. Root development, oxidative stress, IAA content and molecules/enzymes involved in IAA metabolism were analyzed to study the plant response to these treatments. The aims of this work were to assess whether ZnO particles induced alterations in root developmental pattern and IAA concentration of an agronomical relevant plant such as rice and to evaluate whether the action of ZnO particles may depend on their size. Our hypothesis was that eventual changes in root development induced by ZnO particles were mediated by their impact on IAA homeostasis.

RESULTS

The particles of ZnO were previously characterized in Spanò et al (2020). Briefly, NP-ZnO showed a round profile or nearly prismatic shape, with diameters from about 20 to 107 nm. Most of the nanoparticles had diameters in the frequency class 41–50 nm. B-ZnO had predominantly a rod-like shape and sizes varying from 300 to 1 300 nm, with only rare particles with one dimension smaller than 80–90 nm.

Seedling growth

NP-ZnO and B-ZnO at higher concentration (100 mg/L) induced the reduction of root length in comparison with control, where the decreases were of about 18% and 30%, respectively (Table 1), and these reductions corresponded with the higher H_2O_2 (100 mg/L NP-ZnO and B-ZnO) concentrations. In this study, treatments induced an increase in LR density only when ZnO was supplied as B-ZnO and the greatest response was recorded in 100 mg/L B-ZnO, with a 49% increase of LR density in comparison with control (Fig. 1-A). The increase in LR density in these plants coincided with IAA concentration (Fig. 1-B). The response of the coleoptile length changed depending on particle size (Table 1). While B-ZnO slightly reduced the length of coleoptile (although not significantly), NP-ZnO increased it compared with control, and the difference was significant under the lower concentration (10 mg/L) of NP-ZnO. These differences were mirrored in the values of the ratio root length and coleoptile length (Table 1), which was about 24% lower in the seedlings treated with higher concentration of both forms of ZnO in comparison with the control.

Histochemical detection of Zn in roots

In rice treated with NP-ZnO, deep red/brown coloured complexes were clearly detectable in root hairs (Fig. 2-A to -F). In this study, treatment with 10 mg/L B-ZnO did not produce a colour response within root cells (Fig. 2-G and -H). In addition, at 100 mg/L B-ZnO, coloured complexes at the surface of epidermic cells were observable (Fig. 2-I and -J).

Table 1. Lengths of root and coleoptile, and concentrations of hydrogen peroxide, thiobarbituric acid reactive substance (TBARS) and phenol in rice after 7 d of imbibition under different conditions.

Condition	Root length (RL, mm)	Coleoptile length (CL, mm)	Ratio of RL to CL	H_2O_2 concentration (μmol/g)	TBARS concentration (nmol/g)	Phenol concentration (mg/g)
Water	76.49 ± 3.03 a	23.71 ± 0.67 bc	3.22 ± 0.12 a	0.50 ± 0.02 b	12.06 ± 0.14 b	0.35 ± 0.00 b
NP10	85.58 ± 2.59 a	27.28 ± 0.75 a	3.14 ± 0.22 a	0.47 ± 0.07 b	12.84 ± 0.07 a	0.31 ± 0.00 d
NP100	62.80 ± 1.84 b	25.64 ± 0.76 b	2.45 ± 0.04 b	0.72 ± 0.07 a	10.41 ± 0.14 c	0.44 ± 0.01 a
B10	76.27 ± 2.62 a	21.25 ± 0.75 c	3.59 ± 0.24 a	0.49 ± 0.07 b	9.64 ± 0.07 d	0.26 ± 0.00 e
B100	54.25 ± 1.99 b	22.35 ± 0.68 c	2.43 ± 0.03 b	0.61 ± 0.02 ab	10.28 ± 0.14 c	0.33 ± 0.00 c

NP10, 10 mg/L zinc oxide nanoparticle (NP-ZnO); NP100, 100 mg/L NP-ZnO; B10, 10 mg/L bulk counterpart (B-ZnO); B100, 100 mg/L B-ZnO. Data are Mean ± SE (n = 20 for RL, CL and ratio of RL to CL, and n = 4 for H_2O_2, TBARS and phenol concentrations). Different lowercase letters in a column indicate significant differences by the post hoc Tukey test ($P \leq 0.05$).

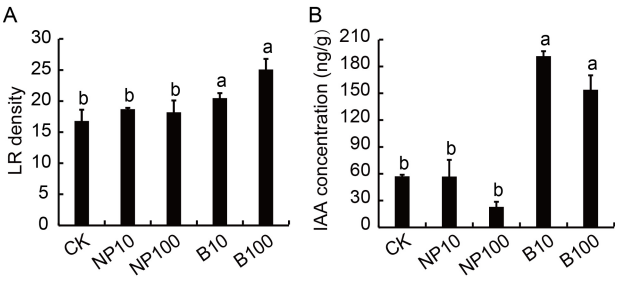

Fig. 1. Lateral root (LR) density (A, expressed as number of LRs/cm) and indole-3-acetic acid concentration (IAA, B) in roots of rice after 7 d of imbibition under different conditions.

CK, Control (water); NP10, 10 mg/L zinc oxide nanoparticle (NP-ZnO); NP100, 100 mg/L NP-ZnO; B10, 10 mg/L bulk counterpart (B-ZnO); B100, 100 mg/L B-ZnO.

Data are Mean ± SE (n = 4). Different lowercase letters above the bars indicate significant differences by the post hoc Tukey test ($P \leq 0.05$).

H_2O_2 and thiobarbituric acid reactive substance (TBARS) concentrations

Treatment with 100 mg/L NP-ZnO induced a significant increase (by 45%) of H_2O_2 concentration, and 100 mg/L B-ZnO also caused a rise of H_2O_2 (by 23%), but it was not statistically significant (Table 1). *In situ* evaluation of H_2O_2, performed on seminal roots, showed that all treatments induced an intense staining, mostly localized in the root apical meristem region (Fig. 3-A). In addition, a strong red staining, extending to differentiation zones, was characterized in 100 mg/L NP-ZnO samples (Fig. 3-A), as confirmed by biochemical analyses (Table 1).

In the present system, however, oxidative damage, estimated as TBARS concentration (Fig. 3-B), was significantly lower than in control in all the treated seedlings, except for the treatment 10 mg/L NP-ZnO, in which this stress parameter showed the highest value (Table 1). The staining pattern obtained by Bodipy probe and related to lipid peroxidation confirms that, following treatments, the root apex of our seedlings was the portion most susceptible to oxidative damage, exhibiting a high sensitivity to Zn (Fig. 3-B).

Endogenous IAA concentration

The concentration of IAA was analyzed in the roots of the studied plants (Fig. 1-B). The amounts of Zn that were administered to rice plants exhibited a positive effect on the level of IAA only when applied as B-ZnO, whereas NP-ZnO did not show any significant effect. The effects of the type of Zn particles on LR density were also assessed. Statistical analyses (Table S1) showed that B-ZnO treatments were significantly different from both NP-ZnO and control, hence only the former increased IAA concentration in roots and promoted LR development.

Phenols, peroxidase (POX) and IAA oxidation activities and electrophoretic POX separation

In this study, there was a general decline of phenol concentration in treated seedlings compared with control, and the lower value was detected under the lower ZnO concentrations (28% and 11% decrease caused by 10 mg/L B-ZnO and 10 mg/L NP-ZnO, respectively, Table 1). The concentration being equal, the lowest contents of these antioxidant molecules

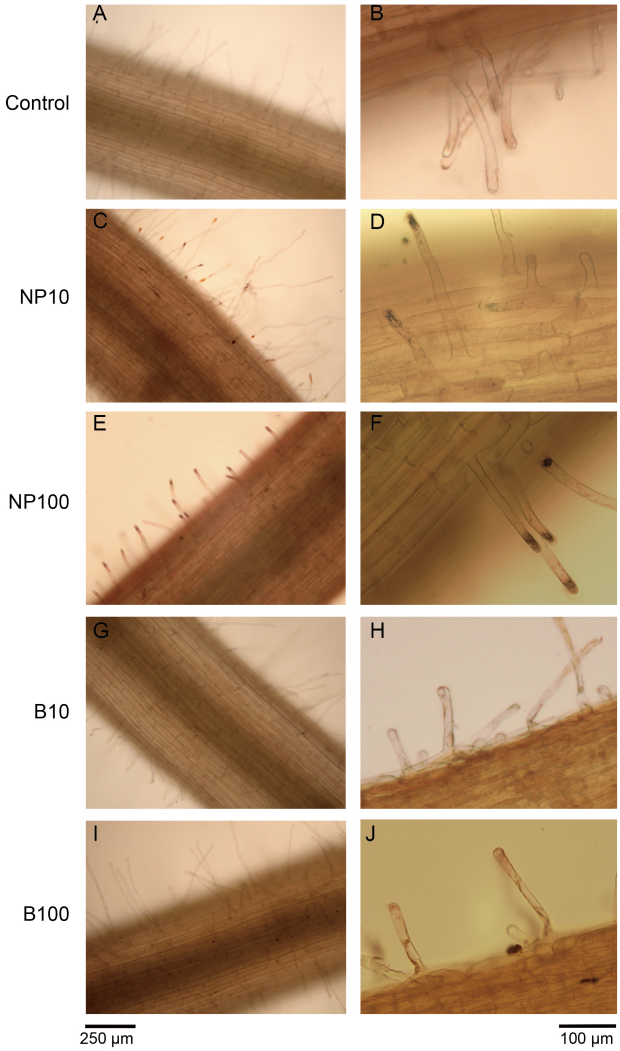

Fig. 2. Histochemical detection of Zn in rice roots of comparable developmental stage after treatment with dithizone.

A and **B,** Control (water); **C** and **D**, 10 mg/L zinc oxide nanoparticle (NP-ZnO); **E** and **F**, 100 mg/L NP-ZnO; **G** and **H**, 10 mg/L bulk counterpart (B-ZnO); **I** and **J**, 100 mg/L B-ZnO. The images on the right side show representative details at higher magnification of the roots on the left side.

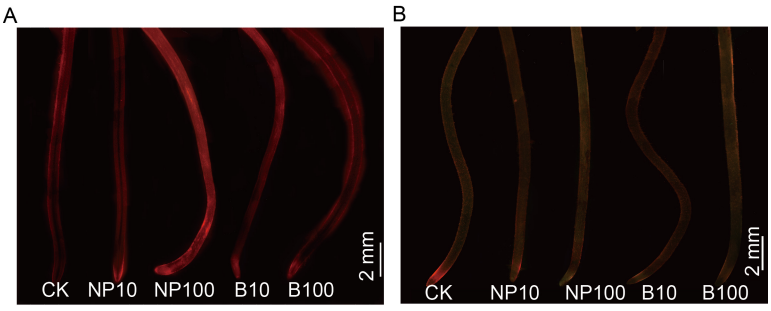

Fig. 3. Histochemical detection of H_2O_2 by amplex ultra-red reagent (A) and lipid peroxidation by bodipy reagent (B).
CK, Control (water); NP10, 10 mg/L zinc oxide nanoparticle (NP-ZnO); NP100, 100 mg/L NP-ZnO; B10, 10 mg/L bulk counterpart (B-ZnO); B100, 100 mg/L B-ZnO.

were recorded under bulk treatments. IAA oxidation activities (Fig. 4-A) were significantly lower under 10 mg/L NP-ZnO than under 100 mg/L NP-ZnO. However, IAA oxidation activities showed no significant difference between 10 and 100 mg/L B-ZnO and between the control and treated materials. Guaiacol POX activities in the studied roots (Fig. 4-B) were significantly lower in 10 mg/L B-ZnO plants and significantly higher in the control. After electrophoresis (Fig. 4-C), specific staining for POX-revealed bands with different mobility, with distinct patterns depending on the treatments. Noteworthy, band 1 was present only in control roots, while bands 2, 3 and 4 were also detectable in NP-treated roots, but not in B-treated roots.

DISCUSSION

Seedling growth

Many data report the toxicity of ZnO for plants, which may undergo disturbance to root development with a negative impact on their growth and morphology (Lin and Xing, 2008; Spanò et al, 2020). Root length, in particular, is a key feature of root morphology, which has an important impact on plant fitness (Meng et al, 2019). The reduction in root length under 100 mg/L B-ZnO and 100 mg/L NP-ZnO (Table 1) is in accordance with data Molnár et al (2020). In fact, a dose-dependent negative action is also recorded in two different species of the genus *Brassica*, in which root shortening is induced by 100 mg/L NP-ZnO (Molnár et al, 2020). A significant inhibition of root elongation was also detected in *Allium cepa* after treatment with 5 and 50 μg/mL NP-ZnO for 36 h, and treated roots appear swollen and friable (Sun et al, 2019). Despite the variability of effects on coleoptile length (Table 1), the ratios of the root length and length coleoptile were significantly lower in treated plants, suggesting that ZnO has the ability to modify the seedling growth habit, with a preferential development of the coleoptile over the root. In accordance, a treatment with 300 mg/L NP-ZnO induced a reduction of this ratio by about 40% in *Arabidopsis* (Wang et al, 2016). LRs have a great importance in root functionality, as they increase its biomass with positive impact on water and nutrient uptake and on anchorage to soil (Jing and Strader, 2019). In addition, the pattern of distribution of LRs is a key characteristic of root architecture and is often considered as an adaptive response to stress conditions (Bellini et al, 2014), such as hypoxia and high concentrations of heavy metals (Potters et al, 2007; Péret et al, 2009; Lavenus et al, 2013). In this study, only the bulk form of ZnO induced an increase in LR density, underlining the importance of particle size in

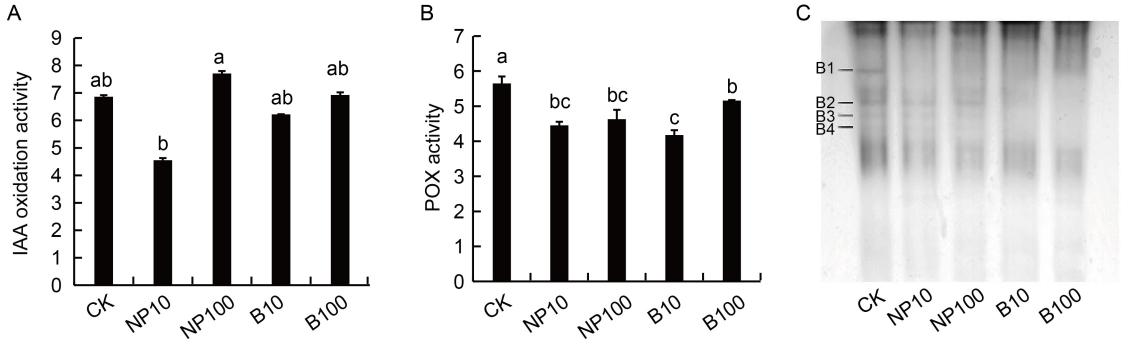

Fig. 4. Indole-3-acetic acid (IAA) oxidation activity (A), guaiacol peroxidase (POX) activity (B) and native polyacrylamide gel electrophoresis of guaiacol peroxidase (C) from rice roots after 7 d of imbibition.
In **A** and **B**, enzymatic activities are expressed as U/mg protein. CK, Control (water); NP10, 10 mg/L zinc oxide nanoparticle (NP-ZnO); NP100, 100 mg/L NP-ZnO; B10, 10 mg/L bulk counterpart (B-ZnO); B100, 100 mg/L B-ZnO.
Data are Mean ± SE (n = 4). In **C**, B1, B2, B3 and B4 represent different bands of enzymatic activity.

the interaction with plants. A crucial role in the regulation of LR development is attributed to auxin (Dubrovsky et al, 2008; Du and Scheres, 2018). In rice, the function of auxin in LR growth is demonstrated by studies on mutants devoid of LRs or with altered LR formation, which are less sensitive to IAA in comparison with wild type (Meng et al, 2019).

Histochemical detection of Zn in roots

Dithizone staining technique has been widely employed for revealing Zn at cellular and tissue levels in different samples (Duarte et al, 2016). The presence of coloured complexes in root hairs under NP-ZnO treatment suggested that NP-ZnO was taken up from the growth medium. This outcome is in accordance with the results of Lin and Xing (2008) which demonstrated the ability of NP-ZnO to penetrate inside root cells. In addition, as stated above, NP-ZnO, by exposing a higher surface area, can release Zn ions (Nemček et al, 2020), which could have been in turn absorbed: this might have contributed to the recorded histochemical response. The absence of colour response within root cells under treatment with B-ZnO (Fig. 2-G, -H, -I and -J) indicated that the size of these particles, larger than the NP-ZnO ones, was a hinder to plant cell barriers overcoming (Medina-Velo et al, 2017), even if root showed some response to the treatment. Indeed, we cannot exclude the possibility that the bulk form also releases Zn ions, but probably in lower amounts than NP-ZnO, and such quantities would not be histochemically detectable. The presence of coloured complexes at the surface of epidermis under higher concentration of the bulk form (Fig. 2-G, -H, -I and -J) suggested that bulk material can alter root growth and function by physical/chemical interaction with the root surface. The results obtained with this Zn-sensing dye led us to hypothesise that the effects elicited by the different treatments on both growth and oxidative stress are attributable, for nano scale material, mainly to a direct interaction with plant cells, linked to the absorption of Zn, while the bulk material can alter root development mostly by acting indirectly, adhering at the root surface.

H_2O_2 and TBARS

The production of ROS, such as H_2O_2, can be induced by NP-ZnO in several plants (Zoufan et al, 2020; Ruiz-Torres et al, 2021). Data in this study confirm these findings, with a significant increase in H_2O_2 concentration under 100 mg/L of both NP-ZnO and B-ZnO treatment.

The overproduction of ROS can induce membrane lipid peroxidation and damage to cellular structures and macromolecules (Parida and Das, 2005). However, in our system, there seemed to be no correlation between the concentration of H_2O_2 and oxidative damage. It must be borne in mind that this molecule, in addition to being involved in oxidative stress, is a ubiquitous signal in morphogenesis and in LR formation (Su et al, 2006).

According to the histochemical approach, which can also display little differences in the pattern of distribution of oxidative stress markers, we can gain further information, which would not be available with biochemical analysis. It was possible in this way to point out that the root apex of our seedlings was the portion most susceptible to oxidative damage. An excess of Zn and the other metals in the growing medium can alter root apex homeostasis due to a ROS imbalance, with consequent oxidative damages (Li et al, 2016). In addition, Zn being a cofactor and an activator of key enzymes and transcriptional factors, changes of its concentration can modify multiple metabolic pathways, including hormone balance and auxin production (Hambidge et al, 2000).

Endogenous IAA

As IAA is the main auxin in rice (Yamamoto et al, 2007), changes of its concentration in the roots of the studied plants in response to Zn application were of particular interest (Fig. 1-B). The interplay between Zn and IAA has also been extensively investigated in rice. Wang et al (2021) have shown that Zn at low concentrations increases the level of IAA in rice roots, whereas higher concentrations of the metal have the opposite effect. In our work, Zn had a positive impact on root IAA levels only when administered as bulk particles. It may be hypothesised that Zn, when supplied as B-ZnO, is absorbed in very low amounts by the root, thus inducing the previously cited increase of IAA. Conversely, NP-ZnO treatments may facilitate the absorption of the element, up to such a point that it may lose the positive effect on IAA level. Eventually, higher concentrations of Zn in root can cause a decrease of IAA.

The development of LRs is a process strictly controlled by auxin, from root initiation to emergence (Malamy and Benfey, 1997). Given this universally acknowledged role of IAA, the effects of the type of Zn particles on LR density have been assessed. Zn

applied as B-ZnO was the sole treatment which elicited a significant effect, therefore the bulk particles of Zn increased both IAA concentration in roots and LR development. These results suggested that B-ZnO particles, at both applied concentrations, enhanced LR development through the rise of IAA in root tissues, thus supporting our working hypothesis.

Phenols, POX and IAA oxidation activities and electrophoretic POX separation

To counteract oxidative damage, plants have evolved an antioxidant machinery, both enzymatic and non-enzymatic. Among molecular antioxidants, phenols, due to their abilities to function as hydrogen donors, reducing agents and singlet O_2 quenchers (Rice-Evans et al, 1997), are powerful scavengers of ROS, also capable of inhibiting enzymes that produce free radicals (Doroteo et al, 2013). They are also involved in IAA metabolism, functioning as protective agents against POX-induced IAA degradation (Krylov and Dunford, 1996; Montanaro et al, 2007). In this study, there was a general decline of phenol concentration in treated plants, with the lowest contents associated with higher IAA concentrations (Fig. 1-B), which apparently does not agree with the role of phenols in IAA protection.

Enzymatic catabolism is generally considered to be a key regulator of the free auxin pool (Normanly et al, 2010; Zhang and Peer, 2017). In our material, however, the absence of particular bands (Fig. 4-C) of POX activity in B-ZnO-treated roots seems to be of particular relevance coinciding with high levels of IAA (Fig. 1-B), and suggesting their possible involvement in the catabolism of this growth regulator.

In rice, ZnO influenced both growth and morphology of roots and changed seedling growth habit, with a prevailing development of the coleoptile over the root. Alterations in the concentration/pattern of localization of oxidative stress markers were also observed, with NP-ZnO eliciting the highest signal of oxidative damage in root meristem apex. Indeed, a different action depending on particle size was recorded. B-ZnO particles, probably leading to a low Zn uptake inside roots, were associated with a significant increase in IAA concentration, in turn related with a rise in LR density. On the contrary, NP-ZnO particles, inducing high levels of Zn inside root cells, did not increase either IAA concentration, or LR density. Therefore, present results support our hypothesis that IAA concentration was regulated more by the catabolism operated by POX than by the protective action of phenols. Since ZnO can induce both morphological and physiological changes in a crop such as rice, care must be taken when introducing it (in particular in the form of nanoparticles) into the environment, to prevent unpredictable adverse effects.

METHODS

Plant material and experimental design

NP-ZnO (size from about 20 to 107 nm) and B-ZnO (size from about 300 to 1 300 nm) were purchased from Sigma Aldrich, USA. Grains of *Oryza sativa* L., var. Cerere (kindly provided by Sardo Piemontese Sementi Soc Coop Soc Agricola, Vercelli, Italy) were surface-sterilized for 15 min in 5% sodium hypochlorite and rinsed, and were then germinated in Petri dishes at 25 ºC ± 1 ºC, in the dark, with a relative humidity of 70%. Total 10 dishes with 30 grains in each have been prepared for control and for each treatment: with water (control) or with a suspension of B-ZnO (10 and 100 mg/L) or NP-ZnO (10 and 100 mg/L). The two ZnO concentrations, below or close to the critical values (Srivastav et al, 2021), were chosen based on preliminary experiments, in which concentrations in the range of 10 to 200 mg/L were used. Under 10 mg/L treatment, there were no significant effects on root growth, while 100 mg/L was the minimum concentration which induced root growth inhibition. At 7 d after treatment, rice seedlings were collected and the lengths of roots and coleoptiles were measured. In addition, four roots were isolated and used for LR density determination. Roots were collected, washed and immediately used for histochemical analyses or fixed in liquid nitrogen and stored at -80 ºC until use for all other analyses. For biochemical parameters, root tissues were obtained from 10 randomly selected plants per treatment.

Determination of LR density

The determination of LR density was performed on four randomly selected plants counting the number of LRs and LR primordia per unit of parent root length (cm) under an optical microscope (Alarcón et al, 2019). Only the segments of parent root with LRs and LR primordia were considered.

H_2O_2 and TBARS determinations

The concentration of H_2O_2 in roots was determined according to Jana and Choudhuri (1982). After grounding and homogenization in phosphate buffer (50 mmol/L, pH 6.5), the homogenate was centrifuged at 6 000 × *g* for 25 min. The concentration of H_2O_2 was determined spectrophotometrically at 410 nm using 0.1% titanium oxysulfate in 20% H_2SO_4 and expressed as μmol/g fresh weight (FW). Calculations were made by referring to a standard curve. Lipid peroxidation in roots was estimated by determining the amount of TBARS, according to Wang et al (2013), with minor modifications as described by Spanò et al (2017). Briefly, samples after mixing

with the TBA reagent (10% trichloroacetic acid + 0.25% thiobarbituric acid) were heated at 95 ºC for 30 min, cooled for 15 min, and centrifuged at 2 000 × *g* for 15 min. The concentration of TBARS was expressed as nmol/g FW and calculated as specific absorbance at 532 nm after subtraction of the nonspecific absorbance at 600 nm.

Histochemical detection of Zn, H_2O_2 and lipid peroxidation

Five roots of comparable developmental stage, randomly selected from control and treated plants, were excised and used for each histochemical detection. *In situ* localization of Zn in control and treated roots was performed by the dithizone (diphenylthiocarbazone) method, as described by Spanò et al (2019). Zn occurrence in plant cells/tissues was detectable as brown/reddish colour precipitates. The selected roots were stained for 1.5 h with a dithizone solution (30 mg dissolved in 60 mL acetone and 20 mL distilled water), thoroughly rinsed in water and immediately analyzed using a Leitz Diaplan light microscope (Leitz microscope, Wetzlar, Germany). Images were captured using a Leica DFC 420 (Leica Microsystems, Heerbrugg, Germany).

Imaging of H_2O_2 and lipid peroxidation levels was carried out by specific fluorescent probes. Amplex UltraRed Reagent (Life Technologies, Carlsbad, USA) was employed for *in situ* H_2O_2 detection (Spanò et al, 2020) as red signal, observed with a fluorescence microscope (568ex/681em nm, Leica DMB, Leica Microsystems, Wetzlar, Germany). BODIPY 581/591 C11 was used as a free radical sensor to visualize lipid peroxidation as a change of the fluorescence emission peak from red to green. Microscope evaluation was performed, acquiring simultaneously the green (485ex/510em nm) and the red fluorescence (581ex/591em nm) signals and merging the two images (Giorgetti et al, 2019).

Extraction and determination of phenols

Phenolic compounds were measured in rice roots according to Arezki et al (2001). After homogenization in 0.1 g/L HCl, centrifugation at 6 000 × *g* for 10 min and incubation at 20 ºC for 3 h, 300 µL of extract were added to 1.5 mL H_2O + 0.1 mL Folin-Ciocalteu reagent and left so for 3 min. After addition of 400 µL Na_2CO_3 (20%), the solution was incubated at 100 ºC for 1 min, cooled in ice bath and the absorbance at 750 nm was recorded. The concentration of phenolic compounds was calculated as equivalent of gallic acid (mg/g FW) on the basis of a standard calibration curve.

IAA analysis

Roots were cut with a scalpel, separated in three replicated samples, and immediately dipped in cold 70% aqueous acetone (1:5). They were homogenized by mortar and pestle and divided into three subsamples. All replicates and subsamples were separately analyzed. Each homogenate was supplemented with a suitable amount of [^{13}C]^{6}IAA (Cambridge Isotope Laboratories, Inc., Andover, MA, USA) as internal standard, then stirred for 4 h at 4 ºC, before centrifugation at 2 000 × *g* for 15 min. The residue was re-extracted twice and the extraction solvents were pooled. The extraction solvents were reduced to the aqueous phase (approximately to a volume of 5 mL), under vacuum at 35 ºC, added with acetic acid (to a final concentration of 0.5%), adjusted to pH 2.8 with 0.1 g/L HCl and loaded on C18 SPE cartridges (Supelco, Milan, Italy), 5 mL volume, previously conditioned with 5 mL methanol and 5 mL of 0.5% acetic acid. Samples were loaded and passed through the phase without drying out. Cartridges were washed with 5 mL of 0.5% acetic acid, followed by 5 mL of 30% methanol + 70% of 0.5% acetic acid. Fractions putatively containing IAA were isolated by eluting the columns with 5 mL of 70% methanol + 30% of 0.5% acetic acid. Column conditioning, washing and IAA elution were carried out at a flow rate of 1 mL/min. The collected fractions were evaporated under reduced pressure, resuspended in a small volume of 20% aqueous acetonitrile containing 0.5% acetic acid and filtered through a 0.45-µm PTFE membrane. They were purified by reverse-phase high performance liquid chromatograph using a Spectrasystem P2000 pump with a Spectrasystem UV1000 detector (Thermo, Waltham, MA, USA) operating at 254 nm wavelength. The instrument was equipped with a Kinetex C18 column, 250 mm × 4.6 mm ID, 5 µm particle size (Phenomenex, Bologna, Italy), eluted at a flow rate of 1 mL/min. Samples were applied to the column and fractions were collected while the column was being eluted with 0.5% acetic acid in 20% acetonitrile. The fraction corresponding to the elution volume of IAA standard was reduced to a small volume and transferred to a capillary tube, dried thoroughly and silylated with bis (trimethylsilyl)trifluoroacetamide containing 1% trimethylchlorosilane (Pierce, Rockford, Illinois, USA). Gas chromatography-mass spectrometry (GC-MS) analysis was performed on a Saturn 2200 quadrupole ion trap mass spectrometer coupled to a CP-3800 gas chromatograph (Varian, Palo Alto, CA, USA) equipped with a MEGA 1 capillary column (MEGA, Legnano, Italy) 25 m × 0.25 mm × 0.25 µm film thickness, coated with 100% dimethylpolysiloxane. The injection was splitless with 2 min purge off, at 250 ºC. The temperature of the transfer line between the gas chromatograph and the mass spectrometer was set at 250 ºC. Oven temperature was 120 ºC for 2 min, followed by a gradient from 120 ºC to 190 ºC at 35 ºC/min, then from 190 ºC to 210 ºC at 6 ºC per min and a final ramp from 210 ºC to 300 ºC at 35 ºC/min with a final hold of 10 min. Full scan mass spectra were obtained in EI+ mode with an emission current of 30 mA, an axial modulation of 4 V and the electron multiplier set at -1500 V. Data acquisition was from 70 to 350 Da at a speed of 1.4 scan/s. The following ions were monitored for IAA analysis: m/z 202 and 319 for IAA, and 208 and 325 for ^{13}C-labelled internal standard. Identification and quantification of the analytes were confirmed by tandem MS, by simultaneous dissociation of the ions 202 for IAA and 208 for ^{13}C-labeled internal standard under a resonant waveform with an excitation amplitude of 0.6 V. Quantification of IAA was carried out by reference to a calibration plot obtained from the GC-MS

analysis of a series of mixtures of the standard hormone with its labelled form. Hormonal results were reported as concentrations of IAA in roots.

Enzyme extraction and assay

Roots were ground in an ice-cold mortar with liquid nitrogen and extracted in phosphate buffer (0.06 mol/L, pH 6.1) containing polyvinylpyrrolidone (1:1) as described by Sorce et al (2017). The homogenate was centrifuged at 10 000 × *g* for 5 min and the supernatant was recovered and used as a crude enzyme extract. Guaiacol POX (EC1.11.1.7) activity was determined according to Arezki et al (2001), using 1% guaiacol as substrate and following the oxidation of guaiacol by H_2O_2 (extinction coefficient 26.6 mmol/L each centimeter) at 470 nm. Enzymatic activity was expressed as U/mg protein, one unit oxidising 1.0 μmol guaiacol per min. IAA oxidation activity was measured as described in Beffa et al (1990) with minor modifications. To the reaction solution (100 μmol/L $MnCl_2$, 50 μmol/L *p*-coumaric acid, 15 μg IAA and 200 μL the extract in 6.66 mmol/L phosphate buffer, pH 6.0) incubated at 24 ºC for 50 min, 2 mL modified Salkowski reagent (Pilet and Lavanchy, 1969) were added. IAA degradation was estimated at 535 nm and expressed as U/mg protein, one unit being equivalent to 1 μg IAA degraded by 1 mL of extract in 50 min. Protein measurement was performed according to Bradford (1976), using bovine serum albumin as standard.

Electrophoretic POX separation

Electrophoresis was performed on 10% PAGE according to Milone et al (2003) and Sorce et al (2017), using 1.5 mol/L Tris-HCl buffer at pH 8.8. Equal amounts (25 μg) of proteins extracted from rice roots were loaded onto electrophoretic gel. After running (200 V, constant current of 35 mA per gel), gels were incubated in 1 mol/L sodium acetate buffer at pH 4.6 containing 0.04% benzidine and 10 mmol/L H_2O_2 (90 min in the dark) and enzymatic activity was appeared as dark brown bands.

Statistical analyses

All data were reported as Mean ± standard error (SE) of four replicates, except for root length and coleoptile length, which were determined by measuring 20 seedlings. Analysis of variance (ANOVA) and post hoc Tukey Honest Significant Difference multiple range test were used to identify statistically significant differences among treatments.

The effects of the treatment (Zn particles) on IAA concentration in roots and on LR density were first probed by two independent one-way ANOVAs, followed by pairwise comparisons by the Tukey test. The data were first checked for normality of distribution, by the Shapiro-Wilk test and homogeneity of variances, by the Levene test. Subsequently, data of IAA and LR density were checked for multivariate normality (by Mahalanobi's distance) and homogeneity of variance-covariance matrix (by Box's test), then analyzed by one-way multivariate analysis of variance, followed by pairwise Hotelling's tests comparison with Bonferroni correction. The explanatory variable was the type of treatment, and the response variables were IAA concentration in roots and LR density. The level of significance for all analyses was $P < 0.05$.

ACKNOWLEDGEMENTS

This study was financed by local funding of the University of Pisa. Authors acknowledge Sardo Piemontese Sementi Soc Coop Soc Agricola, Vercelli, Italy, for kindly providing grains of *Oryza sativa*, var. Cerere.

SUPPLEMENTAL DATA

The following material is available in the online version of this article at http://www.sciencedirect.com/journal/rice-science; http://www.ricescience.org.

Table S1. Results of one-way multivariate analysis of variance and post hoc pairwise Hotelling's tests.

REFERENCES

Alarcón M V, Salguero J, Lloret P G. 2019. Auxin modulated initiation of lateral roots is linked to pericycle cell length in maize. *Front Plant Sci*, **10**: 11.

Ali B, Saleem M H, Ali S, Shahid M, Sagir M, Tahir M B, Qureshi K A, Jaremko M, Selim S, Hussain A, Rizwan M, Ishaq W, Rehman M Z. 2022. Mitigation of salinity stress in barley genotypes with variable salt tolerance by application of zinc oxide nanoparticles. *Front Plant Sci*, **13**: 973782.

Ali S, Rizwan M, Noureen S, Anwar S, Ali B, Naveed M, Abd_Allah E F, Alqarawi A A, Ahmad P. 2019. Combined use of biochar and zinc oxide nanoparticle foliar spray improved the plant growth and decreased the cadmium accumulation in rice (*Oryza sativa* L.) plant. *Environ Sci Pollut Res*, **26**(11): 11288–11299.

Aloni R, Aloni E, Langhans M, Ullrich C I. 2006. Role of cytokinin and auxin in shaping root architecture: Regulating vascular differentiation, lateral root initiation, root apical dominance and root gravitropism. *Ann Bot*, **97**(5): 883–893.

Arezki O, Boxus P, Kevers C, Gaspar T. 2001. Changes in peroxidase activity, and level of phenolic compounds during light-induced plantlet regeneration from *Eucalyptus camaldulensis* Dehn. nodes *in vitro*. *Plant Growth Regul*, **33**(3): 215–219.

Beffa R, Martin H V, Pilet P E. 1990. *In vitro* oxidation of indoleacetic acid by soluble auxin-oxidases and peroxidases from maize roots. *Plant Physiol*, **94**(2): 485–491.

Bellini C, Pacurar D I, Perrone I. 2014. Adventitious roots and lateral roots: Similarities and differences. *Annu Rev Plant Biol*, **65**: 639–666.

Bradford M M. 1976. A rapid and sensitive method for the quantitation of microgram quantities of protein utilizing the principle of protein-dye binding. *Anal Biochem*, **72**: 248–254.

Du Y J, Scheres B. 2018. Lateral root formation and the multiple roles of auxin. *J Exp Bot*, **69**(2): 155–167.

Duarte R F, Prom-u-thai C, Amaral D C, Faquin V, Guilherme L R

G, Reis A R, Alves E. 2016. Determination of zinc in rice grains using DTZ staining and ImageJ software. *J Cereal Sci*, **68**: 53–58.

Dubrovsky J G, Sauer M, Napsucialy-Mendivil S, Ivanchenko M G, Friml J, Shishkova S, Celenza J, Benková E. 2008. Auxin acts as a local morphogenetic trigger to specify lateral root founder cells. *Proc Natl Acad Sci USA*, **105**(25): 8790–8794.

Doroteo V H, Díaz C, Terry C, Rojas R. 2013. Phenolic compounds and antioxidant activity *in vitro* of 6 Peruvian plants. *J Peruvian Chem Soc*, **79**(1): 13–20. (in Spanish with English abstract)

Giorgetti L, Spanò C, Muccifora S, Bellani L, Tassi E, Bottega S, Di Gregorio S, Siracusa G, Sanità di Toppi L, Ruffini Castiglione M. 2019. An integrated approach to highlight biological responses of *Pisum sativum* root to nano-TiO_2 exposure in a biosolid-amended agricultural soil. *Sci Total Environ*, **650**(2): 2705–2716.

Hambidge K M, Cousins R J, Costello R B. 2000. Zinc and health: Current status and future directions. *J Nutr*, **130**: 1437–1446.

Hernandez-Viezcas J A, Castillo-Michel H, Servin A D, Peralta-Videa J R, Gardea-Torresdey J L. 2011. Spectroscopic verification of zinc absorption and distribution in the desert plant *Prosopis juliflora-velutina* (velvet mesquite) treated with ZnO nanoparticles. *Chem Eng J*, **170**(1/3): 346–352.

Jana S, Choudhuri M A. 1982. Glycolate metabolism of three submersed aquatic angiosperms during ageing. *Aquat Bot*, **12**: 345–354.

Jing H W, Strader L C. 2019. Interplay of auxin and cytokinin in lateral root development. *Int J Mol Sci*, **20**(3): 486.

Krylov S N, Dunford H B. 1996. Detailed model of the peroxidase-catalyzed oxidation of indole-3-acetic acid at neutral pH. *J Phys Chem*, **100**(2): 913–920.

Lavenus J, Goh T, Roberts I, Guyomarc'h S, Lucas M, De Smet I, Fukaki H, Beeckman T, Bennett M, Laplaze L. 2013. Lateral root development in *Arabidopsis*: Fifty shades of auxin. *Trends Plant Sci*, **18**(8): 450–458.

Li G J, Kronzucker H J, Shi W M. 2016. The response of the root apex in plant adaptation to iron heterogeneity in soil. *Front Plant Sci*, **7**: 344.

Lin D H, Xing B S. 2008. Root uptake and phytotoxicity of ZnO nanoparticles. *Environ Sci Technol*, **42**(15): 5580–5585.

Lv B S, Yan Z W, Tian H Y, Zhang X S, Ding Z J. 2019. Local auxin biosynthesis mediates plant growth and development. *Trends Plant Sci*, **24**(1): 6–9.

Ma H B, Williams P L, Diamond S A. 2013. Ecotoxicity of manufactured ZnO nanoparticles: A review. *Environ Pollut*, **172**: 76–85.

Malamy J E, Benfey P N. 1997. Organization and cell differentiation in lateral roots of *Arabidopsis thaliana*. *Development*, **124**(1): 33–44.

Medina-Velo I A, Barrios A C, Zuverza-Mena N, Hernandez-Viezcas J A, Chang C H, Ji Z X, Zink J I, Peralta-Videa J R, Gardea-Torresdey J L. 2017. Comparison of the effects of commercial coated and uncoated ZnO nanomaterials and Zn compounds in kidney bean (*Phaseolus vulgaris*) plants. *J Hazard Mater*, **332**: 214–222.

Meng F N, Xiang D, Zhu J S, Li Y, Mao C Z. 2019. Molecular mechanisms of root development in rice. *Rice*, **12**(1): 1.

Milone M T, Sgherri C, Clijsters H, Navari-Izzo F. 2003. Antioxidative responses of wheat treated with realistic concentration of cadmium. *Environ Exp Bot*, **50**(3): 265–276.

Molnár Á, Rónavári A, Bélteky P, Szőllősi R, Valyon E, Oláh D, Rázga Z, Ördög A, Kónya Z, Kolbert Z. 2020. ZnO nanoparticles induce cell wall remodeling and modify ROS/RNS signalling in roots of *Brassica* seedlings. *Ecotoxicol Environ Saf*, **206**: 111158.

Montanaro G, Treutter D, Xiloyannis C. 2007. Phenolic compounds in young developing kiwifruit in relation to light exposure: Implications for fruit calcium accumulation. *J Plant Interact*, **2**(1): 63–69.

Mousavi Kouhi S M, Lahouti M, Ganjeali A, Entezari M H. 2015. Long-term exposure of rapeseed (*Brassica napus* L.) to ZnO nanoparticles: Anatomical and ultrastructural responses. *Environ Sci Pollut Res Int*, **22**(14): 10733–10743.

Nemček L, Šebesta M, Urík M, Bujdoš M, Dobročka E, Vávra I. 2020. Impact of bulk ZnO, ZnO nanoparticles and dissolved Zn on early growth stages of barley: A pot experiment. *Plants-Basel*, **9**(10): 1365.

Normanly J, Slovin J P, Cohen J D. 2010. Hormone biosynthesis, metabolism and its regulation: Auxin biosynthesis and metabolism. *In*: Davies P J. Plant Hormones: Biosynthesis, Signal Transduction, Action. Dordrecht, the Netherlands, Springer: 36–62.

Overvoorde P, Fukaki H, Beeckman T. 2010. Auxin control of root development. *Cold Spring Harb Perspect Biol*, **2**(6): a001537.

Pandimurugan R, Thambidurai S. 2016. Novel seaweed capped ZnO nanoparticles for effective dye photodegradation and antibacterial activity. *Adv Powder Technol*, **27**(4): 1062–1072.

Parida A K, Das A B. 2005. Salt tolerance and salinity effects on plants: A review. *Ecotoxicol Environ Saf*, **60**(3): 324–349.

Péret B, de Rybel B, Casimiro I, Benková E, Swarup R, Laplaze L, Beeckman T, Bennett M J. 2009. *Arabidopsis* lateral root development: An emerging story. *Trends Plant Sci*, **14**(7): 399–408.

Pilet P E, Lavanchy P. 1969. Purification of peroxidase extracts (roots of Lens) with 'auxin-oxidase' activity. *Physiol Veg*, **7**: 19–29. (in French)

Potters G, Pasternak T P, Guisez Y, Palme K J, Jansen M A K. 2007. Stress-induced morphogenic responses: Growing out of trouble? *Trends Plant Sci*, **12**(3): 98–105.

Rajput V D, Minkina T, Fedorenko A, Chernikova N, Hassan T, Mandzhieva S, Sushkova S, Lysenko V, Soldatov M A, Burachevskaya M. 2021. Effects of zinc oxide nanoparticles on physiological and anatomical indices in spring barley tissues. *Nanomaterials*, **11**(7): 1722.

Rice-Evans C, Miller N, Paganga G. 1997. Antioxidant properties of phenolic compounds. *Trends Plant Sci*, **2**(4): 152–159.

Ruiz-Torres N, Flores-Naveda A, Barriga-Castro E D, Camposeco-Montejo N, Ramírez-Barrón S, Borrego-Escalante F, Niño-Medina G, Hernández-Juárez A, Garza-Alonso C, Rodríguez-Salinas P, García-López J I. 2021. Zinc oxide nanoparticles and zinc sulfate impact physiological parameters and boosts lipid

peroxidation in soil grown coriander plants (*Coriandrum sativum*). *Molecules*, **26**(7): 1998.

Sorce C, Montanaro G, Bottega S, Spanò C. 2017. Indole-3-acetic acid metabolism and growth in young kiwifruit berry. *Plant Growth Regul*, **82**(3): 505–515.

Spanò C, Bottega S, Ruffini Castiglione M, Pedranzani H E. 2017. Antioxidant response to cold stress in two oil plants of the genus *Jatropha*. *Plant Soil Environ*, **63**(6): 271–276.

Spanò C, Bottega S, Sorce C, Bartoli G, Ruffini Castiglione M. 2019. TiO_2 nanoparticles may alleviate cadmium toxicity in co-treatment experiments on the model hydrophyte *Azolla filiculoides*. *Environ Sci Pollut Res*, **26**(29): 29872–29882.

Spanò C, Bottega S, Bellani L, Muccifora S, Sorce C, Ruffini Castiglione M. 2020. Effect of zinc priming on salt response of wheat seedlings: Relieving or worsening? *Plants*, **9**(11): 1514.

Srivastav A, Ganjewala D, Singhal R K, Rajput V D, Minkina T, Voloshina M, Srivastava S, Shrivastava M. 2021. Effect of ZnO nanoparticles on growth and biochemical responses of wheat and maize. *Plants-Basel*, **10**(12): 2556.

Su G X, Zhang W H, Liu Y L. 2006. Involvement of hydrogen peroxide generated by polyamine oxidative degradation in the development of lateral roots in soybean. *J Integr Plant Biol*, **48**(4): 426–432.

Sun Z Q, Xiong T T, Zhang T, Wang N F, Chen D, Li S S. 2019. Influences of zinc oxide nanoparticles on *Allium cepa* root cells and the primary cause of phytotoxicity. *Ecotoxicology*, **28**(2): 175–188.

Vimercati L, Cavone D, Caputi A, De Maria L, Tria M, Prato E, Ferri G M. 2020. Nanoparticles: An experimental study of zinc nanoparticles toxicity on marine crustaceans: General overview on the health implications in humans. *Front Public Health*, **8**: 192.

Wang J H, Moeen-ud-din M, Yang S H. 2021. Dose-dependent responses of *Arabidopsis thaliana* to zinc are mediated by auxin homeostasis and transport. *Environ Exp Bot*, **189**: 104554.

Wang X P, Yang X Y, Chen S Y, Li Q Q, Wang W, Hou C J, Gao X, Wang L, Wang S C. 2016. Zinc oxide nanoparticles affect biomass accumulation and photosynthesis in *Arabidopsis*. *Front Plant Sci*, **6**: 1243.

Wang Y S, Ding M D, Gu X G, Wang J L, Pang Y L, Gao L P, Xia T. 2013. Analysis of interfering substances in the measurement of malondialdehyde content in plant leaves. *Am J Biochem Biotechnol*, **9**(3): 235–242.

Yamamoto Y, Kamiya N, Morinaka Y, Matsuoka M, Sazuka T. 2007. Auxin biosynthesis by the *YUCCA* genes in rice. *Plant Physiol*, **143**(3): 1362–1371.

Zhang J, Peer W A. 2017. Auxin homeostasis: The DAO of catabolism. *J Exp Bot*, **68**(12): 3145–3154.

Zhang R C, Zhang H B, Tu C, Hu X F, Li L Z, Luo Y M, Christie P. 2015. Phytotoxicity of ZnO nanoparticles and the released Zn(II) ion to corn (*Zea mays* L.) and cucumber (*Cucumis sativus* L.) during germination. *Environ Sci Pollut Res Int*, **22**(14): 11109–11117.

Zoufan P, Baroonian M, Zargar B. 2020. ZnO nanoparticles-induced oxidative stress in *Chenopodium murale* L, Zn uptake, and accumulation under hydroponic culture. *Environ Sci Pollut Res*, **27**(10): 11066–11078.

(Managing Editor: WANG Caihong)